ADVANCES IN ATMOSPHERIC SCIENCES, VOL. 34, JUNE 2017, 791–803

• **Original Paper** •

# Initial Error-induced Optimal Perturbations in ENSO Predictions, as Derived from an Intermediate Coupled Model

Ling-Jiang TAO[1,2], Rong-Hua ZHANG[*1,2,3], and Chuan GAO[1,2]

[1]*Key Laboratory of Ocean Circulation and Waves, Institute of Oceanology, Chinese Academy of Sciences, Qingdao* 266071*, China*

[2]*University of Chinese Academy of Sciences, Beijing* 10029*, China*

[3]*Laboratory for Ocean and Climate Dynamics, Qingdao National Laboratory for Marine Science and Technology, Qingdao* 266237*, China*

(Received 30 October 2016; revised 18 January 2017; accepted 20 January 2017)

ABSTRACT

The initial errors constitute one of the main limiting factors in the ability to predict the El Niño–Southern Oscillation (ENSO) in ocean–atmosphere coupled models. The conditional nonlinear optimal perturbation (CNOP) approach was employed to study the largest initial error growth in the El Niño predictions of an intermediate coupled model (ICM). The optimal initial errors (as represented by CNOPs) in sea surface temperature anomalies (SSTAs) and sea level anomalies (SLAs) were obtained with seasonal variation. The CNOP-induced perturbations, which tend to evolve into the La Niña mode, were found to have the same dynamics as ENSO itself. This indicates that, if CNOP-type errors are present in the initial conditions used to make a prediction of El Niño, the El Niño event tends to be under-predicted. In particular, compared with other seasonal CNOPs, the CNOPs in winter can induce the largest error growth, which gives rise to an ENSO amplitude that is hardly ever predicted accurately. Additionally, it was found that the CNOP-induced perturbations exhibit a strong spring predictability barrier (SPB) phenomenon for ENSO prediction. These results offer a way to enhance ICM prediction skill and, particularly, weaken the SPB phenomenon by filtering the CNOP-type errors in the initial state. The characteristic distributions of the CNOPs derived from the ICM also provide useful information for targeted observations through data assimilation. Given the fact that the derived CNOPs are season-dependent, it is suggested that seasonally varying targeted observations should be implemented to accurately predict ENSO events.

**Key words**: El Niño predictability, initial errors, intermediate coupled model, spring predictability barrier

**Citation**: Tao, L.-J., R.-H. Zhang, and C. Gao, 2017: Initial error-induced optimal perturbations in ENSO predictions, as derived from an intermediate coupled model. *Adv. Atmos. Sci.*, **34**(6), 791–803, doi: 10.1007/s00376-017-6266-4.

## 1. Introduction

The El Niño–Southern Oscillation (ENSO) is a dominant interannual variability mode in the tropical Pacific, and has been intensively studied over the years (Bjerknes, 1969; Philander, 1983; Zhang et al., 1998; Wang and Fiedler, 2006; Chen et al., 2015) because of its climatic effects and particularly the associated natural disasters (Ropelewski and Halpert, 1987; Ropelewski et al., 1996; Moore et al., 2009). In recent decades, improvements in numerical models have deepened our understanding of its physical mechanism (Battisti, 1988; Wang and Picaut, 2004; Zhang et al., 2008; Zhang and Gao, 2016). Various programs have been conducted to improve our ability to predict ENSO, such as the TOGA (Tropical Ocean–Global Atmosphere) program and the CLIVAR (Climate Variability and Predictability) program. Right now, models can be successfully used to make predictions with a one-year lead time (Zhang et al., 2005b; Chen and Cane, 2008). However, pronounced errors in real-time ENSO predictions still exist (Jin et al., 2008; Luo et al., 2008). For instance, many models incorrectly predicted a warming event in early 2014, and barely forecasted its occurrence in early 2015. Generally, the current prediction skill with regards to ENSO is mainly restrained by the intrinsic limitation of ENSO prediction, incomplete model dynamics (e.g., uncertainties in parameterization schemes), and errors in initial conditions (Toth and Kalnay, 1997). In particular, the role of initial conditions in ENSO prediction has caused extensive concern (Blumenthal, 1991; Goswami and Shukla, 1991; Moore and Kleeman, 1996; Mu et al., 2003). Chen et al. (2004) performed retrospective ENSO forecast experiments and suggested that ENSO prediction capability is significantly dependent on the initial conditions. Zhu et al.

* Corresponding author: Rong-Hua ZHANG
Email: rzhang@qdio.ac.cn

(2012), based on NCEP CFSv2, found that ENSO prediction skill is highly sensitive to the ocean analysis used for initialization. Various approaches have been developed to reveal the relationships between the spatial structure of the initial conditions and the error growth of predictions.

The linear singular vector (LSV) approach has been widely used to determine the optimal initial errors (OIEs) that could invoke the fastest error growth. This approach was first introduced by Lorenz (1965), and promoted the ENSO predictability research carried out by Blumenthal (1991). Subsequently, based on the LSV method, considerable effort has been made to study the OIEs in various ENSO models. As expected, it has been found that the spatial structure of the OIEs is model-dependent. For example, Moore and Kleeman (1996) found that the strong signal of OIEs is confined to the central Pacific. Furthermore, Xue et al. (1997a, 1997b) implemented the LSV approach in the Zebiak–Cane (ZC) model (Zebiak and Cane, 1987), and found a dominant growth structure characterized by an east–west dipole sea surface temperature anomaly (SSTA) mode. In contrast, the OIE patterns were less dependent on the initial time and optimization periods. Additionally, Chen et al. (1997) investigated the sensitivity of OIEs under various reference states in a coupled atmosphere–ocean model (Battisti, 1988), and found that there is only one dominant pattern of OIEs. Recently, Zhou et al. (2008) examined the impact of atmospheric nonlinearities on OIEs. Note that the LSV method assumes linearity for a nonlinear dynamical model; using such a linear theory cannot adequately describe the nonlinear effect.

Given the drawback of the LSV approach, Mu et al. (2003) further extended it to a nonlinear dynamical system and proposed the conditional nonlinear optimal perturbation (CNOP) approach. By analyzing a simple theoretical model (Wang and Fang, 1996), it was found that CNOP-resultant initial errors (CNOPs) could lead to larger error growth than that of the LSV (Mu et al., 2003, 2007a). In particular, Xu (2006) and Yu et al. (2009) detected the spatial distributions of CNOPs using the ZC model and found two types of OIEs: one showed a dipole pattern with negative SSTAs in the equatorial central Pacific and positive anomalies in the eastern Pacific, which plays a role in predicting a large El Niño event in the ZC model; and the other has almost the same pattern but with opposite signs, possessing the potential to predict a weak El Niño. The CNOP-based approach has been successfully used to investigate the spring predictability barrier (SPB) phenomenon, which is notorious as one of the main factors limiting the prediction skill of ENSO (Zebiak and Cane, 1987; Xue et al., 1994; Balmaseda et al., 1995; Webster, 1995; Fan et al., 2000; Samelson and Tziperman, 2001). For instance, Mu et al. (2007b) found that the evolutions of CNOPs in the ZC model are season-dependent and closely related to the SPB. Since CNOPs represent the spatial structure of the fastest possible growing errors, it may be possible to improve the prediction skill of ENSO by filtering the initial CNOP-type errors in the initial conditions. This can be further combined with data assimilation to effectively improve the prediction skill. For example, one way to avoid the appearance of CNOP-type errors is through targeted observations—an observing strategy that aims to identify key regions (sensitive areas) where adding observations may yield a more accurate prediction than doing so in other regions (Mu et al., 2015). As such, observational data in sensitive areas can be more effectively used to constrain the model solution. Indeed, Mu et al. (2014) compared the similarities between the optimal precursors for ENSO and CNOP-type errors in El Niño predictions. It was found that additional observations in the sensitive areas determined by the CNOP approach are able to not only reduce the initial errors, but also better detect the early signals for ENSO events to give relatively accurate predictions. As demonstrated by Chen et al. (1995, 1997), adopting a coupled ocean–atmosphere data assimilation procedure in the ZC model can effectively weaken the SPB phenomenon. It is believed that data assimilation in sensitive areas identified by the CNOP approach provides great potential for effectively improving the prediction skill. Indeed, based on the ZC model and CNOP approach, Yu et al. (2012) divided the tropical Pacific into six parts, and suggested that the central and eastern Pacific regions are the sensitive areas for ENSO prediction in the ZC model. They further demonstrated that implementing additional SST observations in these regions can improve the ENSO prediction skill. However, when using another coupled model, Morss and Battisti (2004a, 2004b) suggested that the most effective regions for data assimilation are in the southeastern and western equatorial Pacific. Thus, the sensitive areas for effective data assimilation can be model-dependent. Given the high cost of oceanic observations in providing the initial conditions for ENSO prediction, identifying a sensitive area to maximize the prediction skill has great economic value, and the CNOP approach offers a way to achieve this.

At present, ENSO predictions are strongly model-dependent, exhibiting wide spread across various coupled models; see http://iri.columbia.edu/our-expertise/climate/forecasts/enso/current. The above-discussed CNOP analyses for ENSO prediction were mostly performed using the ZC model; thus, the insight gained into the relationships between error growth and the spatial structure of the initial conditions may not apply in other models. Due to the model dependence, the spatial characteristics of errors in the initial conditions derived from the ZC model can differ from those derived from other models. There is a clear need to examine the extent to which the CNOP approach can also provide useful information on how to improve ENSO prediction in other coupled models.

In this study, we use a relatively new intermediate coupled model (ICM; Zhang et al., 2003) to perform the CNOP-based analyses. This ICM has been widely used for various modeling studies (Zhang et al., 2008; Zhang and Gao, 2016; Gao and Zhang, 2017), and is also one of the real-time ENSO prediction models used at the IRI of Columbia University for routine monthly assessments. In particular, this model can successfully reproduce the "double dip" evolution of SSTAs in 2010–11 (Zhang et al., 2013). Nevertheless, systematic biases still exist in the prediction of SSTAs for the tropical Pa-

cific (Zhang et al., 2005b). A strong SPB in the model might be related to its initialization scheme, i.e., observed SST data are only applied during model initialization. Recent studies have suggested that the relationship between the thermocline and SST exhibits strong seasonality, being weakest in spring (Zhu et al., 2015a). Correspondingly, the SST-derived subsurface thermal condition is the least accurate during spring (Zhu et al., 2015b). To improve the prediction skill, Gao et al. (2016) implemented a four-dimensional variational (4D-Var) data assimilation method into the ICM, including the development of the adjoint component of the ICM. In the present study, the CNOP approach was adopted to further investigate in this ICM the spatial structure of the errors in the initial conditions and its relationship with ENSO prediction.

A number of questions will be addressed in detail in this paper: What kinds of initial errors can cause significant prediction errors in the ICM? Do the CNOPs in the ICM have the same pattern as those in the ZC model? If so, how do these errors evolve and what are the relevant dynamics? Does the error growth of the CNOPs show obvious seasonal dependence and cause the SPB of ENSO? And what kind of important information can be provided for targeted observations and data assimilation?

Following the introduction, section 2 describes the ICM. In section 3, the details of the CNOP approach are introduced. The CNOPs derived from the ICM are described in section 4, followed by the CNOP-induced error evolutions in section 5. Section 6 compares the CNOPs with those of the ZC model and discusses the implications. And lastly, a conclusion and further discussion are provided in section 7.

## 2. Model description and prediction errors

The following is a brief introduction to the ICM developed by Zhang et al. (2003), which consists of a statistical atmospheric model, an intermediate dynamic ocean model, and an SST anomaly model embedded with an empirical model for the temperature of subsurface waters entrained into the mixed layer ($T_e$). The statistical atmospheric model is constructed from an SVD analysis, in which the covariance matrix is calculated from a time series of monthly mean SST and wind stress (Tau) fields. The observational SST data are from Reynolds et al. (2002), and the Tau data are from the ensemble mean of 24-member ECHAM4.5 simulations, forced by the observed SSTA during the period 1950–99.

The intermediate dynamic ocean model, established by Keenlyside and Kleeman (2002), is mathematically divided into linear and nonlinear components. The linear component is taken from McCreary's (1981) baroclinic model, but with an extension to have a horizontally varying background stratification. The nonlinear component is a highly simplified model described by residual nonlinear momentum equations; this component is concerned with corrections to the solution, which is broken down by the linear assumption.

A fully nonlinear SSTA model, which is embedded into the dynamic ocean model, represents thermodynamic ocean processes over the surface mixed layer. The model equation can be written as

$$\begin{aligned}\frac{\partial T'}{\partial t} = & -u'\frac{\partial \overline{T}}{\partial x} - (\bar{u}+u')\frac{\partial T'}{\partial y} - v'\frac{\partial \overline{T}}{\partial y} - (\bar{v}+v')\frac{\partial T'}{\partial y} \\ & -[(\bar{w}+w')M(-\bar{w}-w') - \bar{w}M(-\bar{w})]\frac{(\overline{T_e}-\overline{T})}{H} \\ & +\frac{\kappa_h}{H}\nabla_h\cdot(H\nabla_h T') + \frac{2\kappa_v}{H(H+H_2)}(T'_e - T') \\ & -(\bar{w}+w')M(-\bar{w}-w')\frac{(T'_e - T')}{H} - \alpha_T T' , \end{aligned} \tag{1}$$

where $T'$ and $T'_e$ are the anomalies of SST and $T_e$, and the overbar of each variable denotes the seasonally varying mean of each parameter [detailed meanings of the variables can be found in Keenlyside (2001)]. Note that the parameterization of $T_e$ is the key factor representing the thermocline feedback. An empirical $T_e$ model is constructed to insert into the SST anomaly model. Two steps are included in deriving the empirical $T_e$ model: first, an inverse modeling of $T_e$ is used to determine the historical $T_e$ using an SST anomaly model when given the other terms, such as the observed SST and velocity field; and second, a relationship between sea level (SL) and $T_e$ is established by an SVD from the historical $T_e$ and SL data. When given an SL anomaly (SLA), $T_e$ anomalies can be optimally determined to calculate the SSTA. The model region only covers the tropical Pacific, covering (33.5°S–33.5°N, 124°–30°E). It has a 2° zonal grid spacing and a meridional grid stretching from 0.5° within 10° of the equator to 3° at the meridional northern and southern boundaries. Readers can find more details on the ICM in Zhang et al. (2005a).

The ICM can successfully depict a dominant four-year oscillation period of SST variability, and has been used to make retrospective ENSO predictions. Correlation analysis between observed and simulated SSTAs at 12-month lead times during 1984–2004 was performed to demonstrate the prediction skill of the ICM. The result is displayed in Fig. 1. It can be seen that the high prediction skill is located in the central and eastern equatorial Pacific (e.g., the maximum value of correlation is larger than 0.6 between 180°W and 150°W), even at the 12-month lead time. The forecasting skill drops rapidly off the equator and near the western Pacific. Webster and Yang (1992) suggested that ENSO predictability is greatly limited by the SPB. As with other ENSO models, the SPB is strong in the ICM (Zhang et al., 2005b). Figure 2a displays anomaly correlations between the observed and predicted monthly Niño3.4 SSTA during the period 1984–2004. A rapid decrease in correlation coefficients can be seen, from 0.9 to 0.6, across April. Accompanied by the SPB phenomenon, an obviously strong growth tendency of prediction errors occurs in early spring (April and May) and summer (July, August and September). Mu et al. (2007a) attributed the SPB to the combined effects of the annual cycle of the mean state, the structure of El Niño, and the pattern of the initial errors by using the CNOP method in the ZC model. Thus, the following question arises: Can the SPB phenomenon be explained by CNOP-type errors in the ICM, regardless of

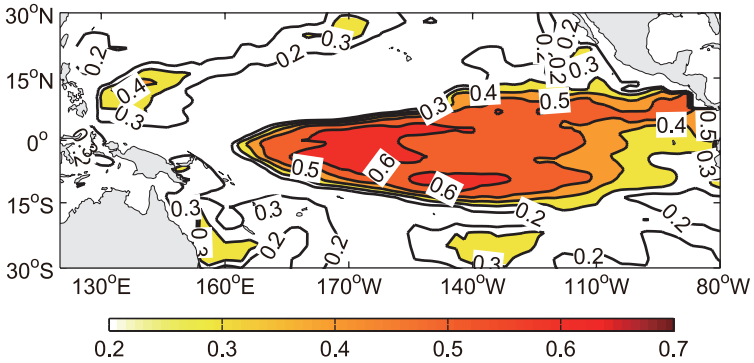


**Fig. 1.** Horizontal distribution of anomaly correlations between the observed and predicted monthly SSTA at 12-month lead times during 1984–2004. Regions with an index of more than 0.3 are shaded in 0.1 intervals.

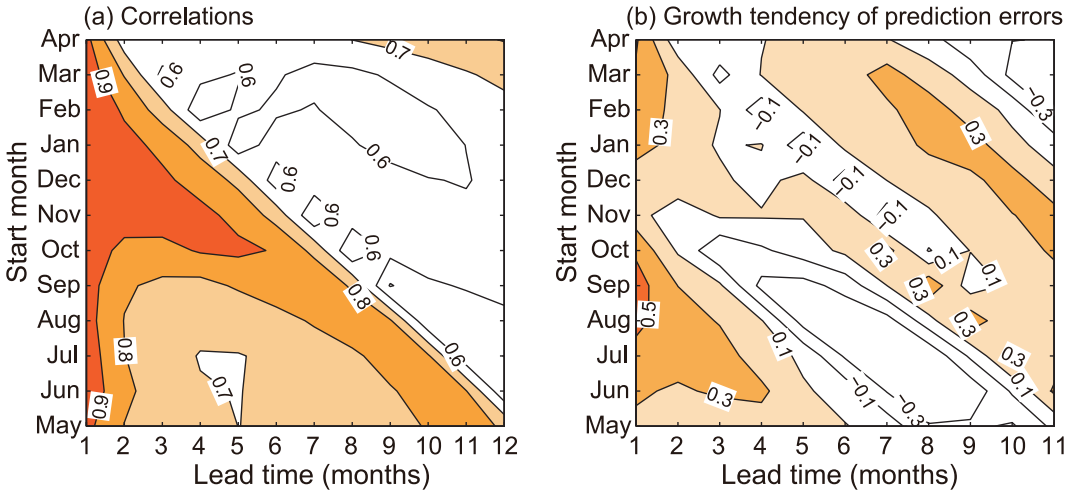


**Fig. 2.** (a) Anomaly correlations between the observed and predicted monthly Niño3.4 SSTA during the period 1984–2004, and (b) the growth tendency of prediction errors for the Niño3.4 index, as a function of start month and lead time. The contour interval is 0.1 for (a) and 0.2 for (b). The correlations more then 0.7 are shaded in (a) and the growth tendencies more than 0.1 are shaded in (b).

the uncertainties of the numerical model and stochastic wind forcing (Zhang et al., 2008)? Next, we report our application of the CNOP approach in the ICM and attempt to identify its OIE structures, as well as its sensitive areas.

## 3. The CNOP approach and analysis procedure

### 3.1. *Brief overview of the CNOP approach*

The CNOP approach was first formulated by Mu et al. (2003) and was introduced to study ENSO predictability, targeted observations of high-impact oceanic–atmospheric environmental events (Mu et al., 2015), and so on. The specific implementation is as follows:

Each model of the atmosphere or ocean can be symbolically written as an initial-value problem:

$$\begin{cases} \dfrac{\partial \boldsymbol{X}}{\partial t} + \boldsymbol{F}(\boldsymbol{X}) = 0 \\ \boldsymbol{X}|_{t=0} = \boldsymbol{X}_0 \end{cases}, \tag{2}$$

where $\boldsymbol{X}(\boldsymbol{x},t) = [X_1(\boldsymbol{x},t), X_2(\boldsymbol{x},t), X_3(\boldsymbol{x},t), \ldots]$ represents state variables (e.g., ocean current, SL, SST, etc.), $\boldsymbol{F}(\boldsymbol{X})$ is a nonlinear operator of the numerical model, and $\boldsymbol{X}_0$ is the initial state. Thus, after the integration time $T$, the solution to Eq. (1) can be defined as

$$\boldsymbol{X}(\boldsymbol{x},T) = \boldsymbol{\mathcal{M}}(\boldsymbol{X}_0)(T)\,, \tag{3}$$

where $\boldsymbol{\mathcal{M}}$ is a propagator governed by the integration time and initial conditions, which, in the physical sense, denotes propagation of the initial physical variable to the future time $T$. By adding perturbation $\boldsymbol{u}_0$ to the initial state, we can obtain a new solution to Eq. (2):

$$\boldsymbol{Y}(\boldsymbol{x},T) = \boldsymbol{\mathcal{M}}(\boldsymbol{X}_0 + \boldsymbol{u}_0)(T)\,. \tag{4}$$

By subtracting from the original solution, the nonlinear growth of variables induced by the initial perturbations can be obtained. To measure the magnitude of $\boldsymbol{Y}(\boldsymbol{x},T) - \boldsymbol{X}(\boldsymbol{x},T)$, an L2 norm square is generally chosen as follows:

$$J(\boldsymbol{u}_0) = \|\boldsymbol{\mathcal{M}}(\boldsymbol{X}_0 + \boldsymbol{u}_0)(T) - \boldsymbol{\mathcal{M}}(\boldsymbol{X}_0)(T)\|^2\,. \tag{5}$$

$J(\boldsymbol{u}_0)$ is called the object function. Note that perturbations satisfy constraint conditions $\|\boldsymbol{u}_0\| \leqslant \delta$. We call the perturbation $\boldsymbol{u}_0^*$ CNOPs if, and only if, they satisfy the following relation:

$$J(\boldsymbol{u}_0^*) = \max_{\|\boldsymbol{u}_0\| \leqslant \delta} J(\boldsymbol{u}_0) \,. \tag{6}$$

To obtain $\boldsymbol{u}_0^*$, the non-monotone spectral projected gradient (SPG2) method is employed to search for the optimal solution in the constrained problem, in which the object function and its gradient with regard to the initial perturbation $\boldsymbol{u}_0$ and constraint condition should be provided; an adjoint model of the original physical model is required to effectively calculate the gradient of the object function. Details on the SPG2 method can be found in Birgin et al. (2000). It should be stressed that, since the high-dimensional control variables cause large amounts of computation, an adjoint model is one of the best ways to acquire the first-order variational of $J(\boldsymbol{u}_0)$.

### 3.2. *Analysis procedure*

We used the CNOP approach to identify CNOPs in the ICM, which could depict ENSO cycles in its extended time integration. Three typical virtual El Niño events simulated in the ICM were selected as reference states for the experiments, denoted as ENSO-1, ENSO-2 and ENSO-3 respectively. Figure 3 presents the evolution of the Niño3.4 index for the corresponding El Niño events. For convenience, the onset phase of El Niño is marked as year(0), and the year before and after the onset phase is marked as year(−1) and year(1), respectively. Likewise, year(1) is the decay phase of El Niño. For the purpose of discussing error evolution during the spring, each idealized prediction experiment was designed to cross through this season in the onset or decay phase. Therefore, we made 12-month predictions in numerical experiments, at monthly intervals, from a start time of July(−1) [i.e., July in year(−1)] to June(1) [i.e., June in year(1)], by superimposing the initial errors on three reference states in each initial calendar month. Thus, $24 \times 3$ sets of time series of predicted SSTAs were obtained. To identify the optimal initial perturbations that invoked the largest deviation from the reference state at the end time of the prediction, the CNOP approach (section 3.1) was executed. Furthermore, an adjoint model of the ICM was required to calculate the gradient of the object function, which has been recently developed and used in 4D-Var data assimilation (Gao et al., 2016). To discuss the effect of the combined initial errors of SSTAs and SLAs, we assume that there were only initial errors in SST and SL at each start month. That is, the initial error field consists of two components: SST and SL, which were computed simultaneously using the CNOP analysis.

Since the model grid was uneven (mentioned in section 2), an area-weighted function was artificially embedded into the constraint and object function. Afterwards, we defined the constraints

$$\delta_1 = \sqrt{\frac{\sum_{i,j} \omega_{i,j}[E_{\mathrm{SST},0}(i,j)]^2}{\sum_{i,j} \omega_{i,j}}} \,, \tag{7}$$

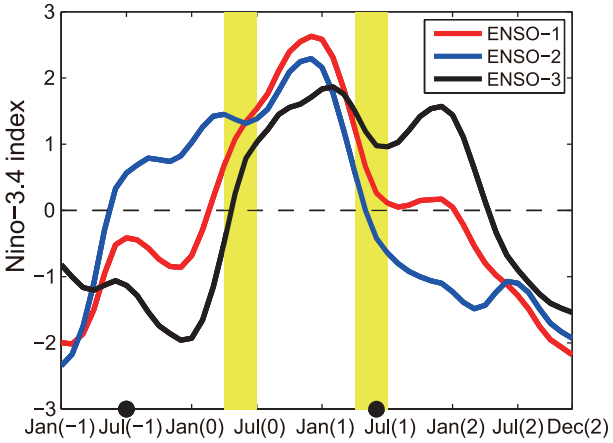


**Fig. 3.** Temporal evolution of the Niño3.4 index for three reference ENSO events (referred to as ENSO-1, ENSO-2, ENSO-3) modeled by the ICM. The colored curves denote the corresponding ENSO (refer to the legend in the top-right corner of the figure), which are chosen to be "true" states as comparisons with prediction experiments. The notation (−1) denotes the year before the ENSO event, (0) denotes the year of the ENSO onset phase, and (1) represents the following year. The spring season, when there is a sharp drop-off in the correlation between predictions and observations associated with ENSO, is represented by yellow bars. The times between the black points are the start months of predictions over the period from July (−1) to June (1), with a one-month interval.

and

$$\delta_2 = \sqrt{\frac{\sum_{i,j} \omega_{i,j}[E_{\mathrm{SL},0}(i,j)]^2}{\sum_{i,j} \omega_{i,j}}} \,, \tag{8}$$

in which $E_{\mathrm{SST},0}(i,j)$ represents the initial errors of the SST at different grid points $(i,j)$, which is the model grid point in the tropical Pacific (31°S–31°N, 124°E–80°W), and $E_{\mathrm{SL},0}(i,j)$ denotes that of SL; $\omega_{i,j}$ is an area-weighted function of the grid point [e.g., if grid (31, 11) has the resolution $2° \times 0.5°$ (lat×lon), then $\omega_{31,31} = 2 \times 0.5$]. Then, the constraint radius ($\delta_1$ and $\delta_2$) represents the maximal initial error per unit area. To measure the initial-error-induced uncertainty of thermodynamics, the object function was defined by

$$J = \sum_{i,j} \omega_{i,j}[E_{\mathrm{SST}}(i,j,t)]^2 \,, \tag{9}$$

where

$$E_{\mathrm{SST}}(i,j,t) = A_{\mathrm{SST},m}(i,j,t) - A_{\mathrm{SST},r}(i,j,t) \,, \tag{10}$$

in which $A_{\mathrm{SST},r}(i,j,t)$ is the reference SSTA at $t$ month and $A_{\mathrm{SST},m}(i,j,t)$ is the modeled SSTA when adding initial errors. Then $E_{\mathrm{SST}}(i,j,t)$ denotes the initial-error-induced SST perturbation for a $t$-month lead-time prediction. Note that the spatial patterns of CNOPs are the same except for the magnitude in the context of various constraint radiuses (Mu et al., 2003; Xu, 2006). Large values of constraints lead to unrealistic initial errors that are considerably larger than practical observational errors. Likewise, undersized initial errors

fail to develop large enough errors to influence the prediction skill. Experientially, the presented results follow the constraints $\delta_1 = 0.16°C$ and $\delta_2 = 0.9$ cm.

## 4. Horizontal distribution of seasonal CNOPs

As mentioned above (section 3), $24 \times 3$ CNOPs were obtained with different start times among the three reference El Niño events for SSTAs and SLAs. By investigating their spatial structures obtained using the CNOPs from the various initial times, we found the CNOPs derived from the same start season to be quite similar. That is, the CNOPs are highly sensitive to the season, rather than the phase of the reference ENSO. With the aim being to identify seasonal OIEs that could induce the largest prediction uncertainties, a composite analysis was implemented among each season for the SSTA and SLA CNOPs. The composites of CNOPs for SSTAs and SLAs derived from various seasons are shown in Fig. 4. Although they look somewhat similar, obvious differences exist between different seasonal CNOPs, especially for the SSTA component. The details are presented in the following two subsections.

### 4.1. *CNOP-type errors of SSTA*

Generally, negative anomaly signals can be clearly seen near the dateline in the equatorial Pacific among the four seasonal SSTA CNOPs (Fig. 4a). However, the structures off the equator are totally different. The summer-type SSTA CNOPs show large-scale negative values near the dateline in the central Pacific, almost covering the Niño3 and Niño4 areas. In

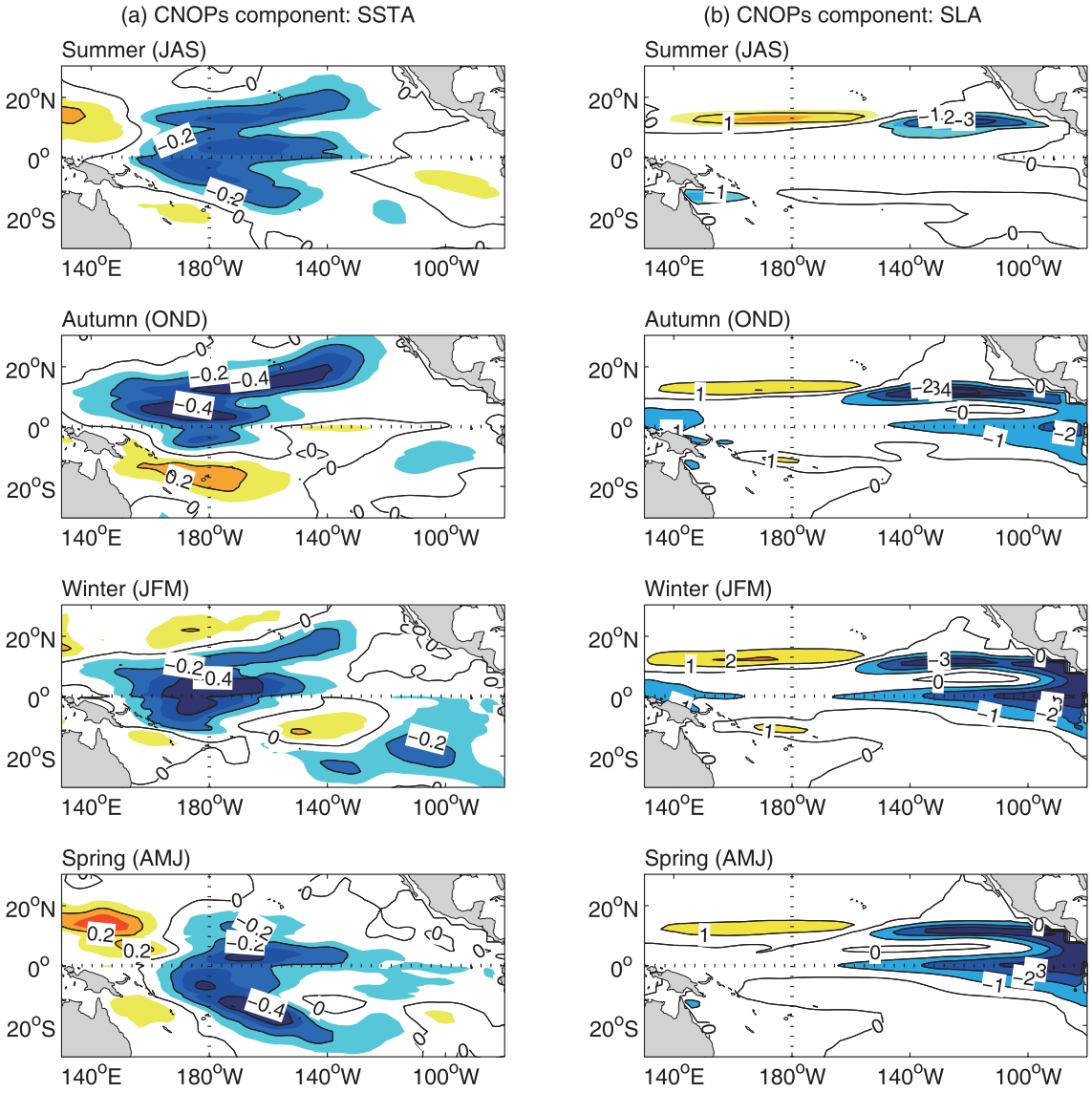


**Fig. 4.** Horizontal distribution of CNOP-type initial errors for (a) SSTA and (b) SLA. It is found that the CNOPs derived from the ICM are significantly season-dependent, but independent of ENSO variability and its phase. The mean of the CNOPs in each season is shown from the top row to the bottom row. The contour interval is 0.1°C for the SSTA and 1 cm for the SLA.

contrast, the autumn type shows a dipole pattern near the dateline, with negative values in the north tropical and equatorial Pacific and positive values in the south tropical Pacific. In winter, the optimal SSTA errors are similar to the summer pattern but much more localized in the central Pacific. The spring SSTA CNOPs exhibit a dipole-like pattern, as with the autumn one, but the signal is located in the north of the western equatorial Pacific with positive anomalies and the south of the central equatorial Pacific with negative anomalies.

### 4.2. *CNOP-type errors of SLA*

The SL represents the subsurface signal and thermal capacity in the tropical Pacific in some ways. Likewise, the CNOP-type errors of the SLA can further explain the effect of the subsurface signal on prediction skill. As shown in Fig. 4, the optimal initial perturbations of the SLA are relatively less sensitive to the season, as compared with the CNOP-type errors of SSTA. The four SLA CNOP types have the same characteristic pattern along 10°N, sharing a kind of seesaw-like structure, with a positive value in the west and a negative value in the east. Additionally, the distinction is located in the eastern equatorial Pacific: a weak positive signal is present in summer, while a strong positive signal is found for the other seasonal SLA CNOPs.

These patterns for SSTAs and SLAs represent errors in the initial conditions that will most likely produce the largest error growth in the prediction. Note that combinations of initial error fields can induce large prediction uncertainties in a nonlinear way at a 12-month lead time. Although there are similarities among the four seasonal SSTA or SLA CNOPs, the combination of the two is significantly dependent on the season, separately referred to as the summer, autumn, winter and spring CNOPs.

## 5. Error evolution

Having displayed the spatial structure of the seasonally varying CNOPs that cause the largest error growth, we next illustrate the temporal evolutions of the CNOP-induced errors within a prediction period.

We adopted the three initial reference states and performed a series of 12-month predictions from a start time of July(−1) to June(1) by integrating the ICM for 12 months (Fig. 3) with the corresponding seasonal CNOPs added. For example, when the initial forecast time was July(−1), the summer CNOPs were superimposed on the initial reference state to form the initial conditions for the following predictions. Through subtraction of the corresponding reference state from the prediction fields, the initial-error-induced evolution was determined, including that of the SSTA, SLA, $T_e$ and Tau.

Figure 5 displays the object function at the end of the prediction as a function of start month according to the three reference ENSO states. As we can see, the error characteristics at the end time prediction induced by the various seasonal CNOPs are quite different. The winter CNOP-induced error growth is largest among the four seasonal CNOPs. Such a

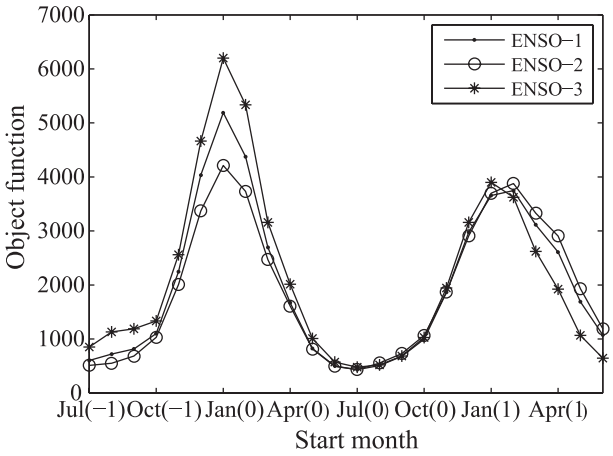


**Fig. 5.** Values of the object function at the end of the prediction as a function of the start month when adding the respective CNOP-type errors in the initial conditions. The results for the three reference ENSO states are shown: line with dots for ENSO-1; line with circles for ENSO-2; line with asterisks for ENSO-3.

difference can be easily understood because ENSO tends to peak in winter. Besides, it also implies that the stability of the predicted SSTA is sensitive to the season, which is accompanied by the so-called SPB phenomenon. In order to study the time-dependent evolution of the CNOPs, the error growth tendencies were calculated and defined as follows:

$$\tau_{t_1} \approx \frac{\sqrt{\sum_{\Omega} \omega_{i,j}[E_{\mathrm{SST}}(i,j,t_2)]^2} - \sqrt{\sum_{\Omega} \omega_{i,j}[E_{\mathrm{SST}}(i,j,t_1)]^2}}{t_2 - t_1}, \tag{11}$$

where $E_{\mathrm{SST}}(i,j,t_1)$ denotes the monthly errors after a leading $t_1$-month prediction, and $\Omega$ denotes the Niño3.4 area. The results are shown in Fig. 6. A strongly season-dependent error growth tendency arises, and this is also similar to the realistic prediction (Fig. 2b) with the largest error growth tendencies appearing during the prediction from May to September. Thus, we consider that the SPB is likely induced by the initial errors of specific structures (i.e., CNOP-type errors). In addition, compared with onset-phase prediction, a relatively weak SPB induced by CNOP-type errors is found during decay-phase prediction, which is accompanied by a relatively weak object function (Fig. 5). This may well explain the fact that the ICM possesses high skill in predicting El Niño during the decay phase, but weak skill during onset-phase prediction.

By tracing the error evolutions, we find that these seasonal CNOPs tend to evolve into a La Niña-like mode. That is, the evolution of each seasonal CNOP has the same dynamics as those of ENSO itself. In terms of the forecast, this indicates that when the initial conditions contain CNOP-like errors, the model tends to predict a weak El Niño event, neutral conditions, or a La Niña event, based on different reference states and amplitudes of CNOPs. In Fig. 7 we separately show the evolutions of CNOP-induced SSTAs as examples for the CNOPs of summer, autumn, winter and spring. It can

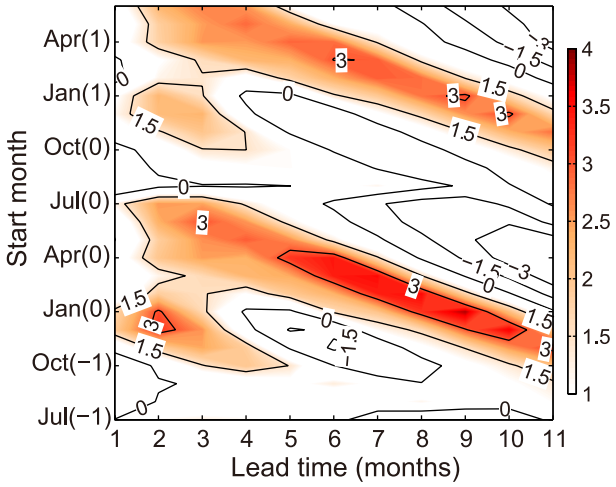


**Fig. 6.** Growth tendencies of prediction errors when imposing CNOP-type errors into the initial conditions as a function of the start month and lead time. The positive tendencies (i.e. larger than 1) are shaded. The result indicates dependence of the evolving CNOPs on the calendar month. The growth tendencies more than 1 are shaded and the contour interval is 1.5.

be seen that error signals first emerge in the central Pacific and then propagate eastwards to the eastern Pacific with enhanced amplitude.

Considering that we found each seasonal CNOP-induced error growth to be different, the next step, naturally, was to try to understand why. Figure 8 displays the CNOP-induced error evolutions of the zonal wind stress anomaly (Taux), $T_e$ anomaly, and SLA. In summer, the CNOP-type errors of SSTA are localized in the central Pacific. An opposite sign of zonal wind errors across 180° along the equator at the start time (Fig. 8a1) is clearly seen as the response of summer CNOPs through air–sea coupling. In addition, the anomalous convergence induced downwelling in the eastern Pacific acts against the SSTA signal. Seasonally, the ocean tends to be in a stable state during the early autumn and fails to enlarge the error growth at the end of prediction. As a result, the SSTA signal almost disappears (Fig. 7a, lead 3). Later, prolonged easterly anomalies trigger uplifted Kelvin waves in the western Pacific and restore the negative signal near the dateline. The error signal is then carried to the eastern Pacific by Kelvin waves. In other words, the summer CNOP-induced errors undergo a transition from a warm to a cold effect. For the autumn CNOPs, Kelvin waves are induced quickly when disturbing the ocean state at the start time. Three months later, SSTA signals propagate into the central and eastern Pacific (Fig. 7b, lead 3) via Kelvin waves. The easterly wind anomaly, negative SSTA and lifted thermocline perturbations over the central and eastern equatorial Pacific establish a Bjerknes-like positive feedback, which causes large prediction errors at the end time of prediction. Figures 8a3, b3 and c3 illustrate the error evolutions induced by winter CNOPs. The dynamics of error growth are the same as those of autumn CNOPs; however, there is stronger positive feedback and a strong induction of large-scale zonal wind anomalies covering the central tropical Pacific after a lead time of five months (i.e., in late spring). That is, the SST variability is in an unstable mode during spring and summer, which gives rise to the SPB phenomenon. However, when adding spring CNOPs, the error signal moves quickly to the eastern Pacific via wave dynamics. The persistence of negative wind errors causes water convergence in the western Pacific and divergence in the eastern Pacific. Additionally, $T_e$ signals appear as byproducts of the strengthened thermocline in both the eastern and western Pacific (but with opposite signs). After a lead time of nine months, the positive feedback process fails to maintain strong westerly wind anomalies in the western Pacific. Kelvin waves are then triggered in the western Pacific, with the potential to erase the signal in the eastern Pacific.

Although CNOPs are sensitive to the initial month, their evolution can be explained by the Bjerknes-like positive feedback and thermocline feedback. SST variability tends to be in a stable mode during the transition between summer and autumn, but an unstable mode during spring and summer, which generates the seasonal dependence of the error growth. That is, the SPB phenomenon in the ICM is likely induced by CNOP-type errors in the initial conditions.

## 6. Comparison with CNOPs derived from the ZC model

As analyzed above, CNOPs derived from the ICM model are apparently different from those derived from the ZC model. Yu et al. (2009) used the CNOP approach to demonstrate the spatial structure of the OIEs of SST and thermocline depth in the ZC model. Unlike that from the ICM, two types of CNOPs are obtainable from the ZC model, which are sensitive to the phase of El Niño. One type possesses an SSTA structure that is characterized by a dipole pattern, with a negative SSTA located in the central equatorial Pacific and a positive one in the eastern Pacific, and a thermocline depth anomaly pattern that is characterized by a positive anomaly along the equator. The other type has a similar pattern but with opposite signs. The former CNOP-type errors, which are mostly derived from the start time of the decay phase of El Niño, tend to induce an El Niño-like error evolution, whereas the latter, which is mostly derived from the onset phase of El Niño, tends to induce La Niña-like error evolution. To some extent, the SLA is equivalent to the thermocline depth anomaly, which also represents the heat content in the upper ocean. In contrast, the optimal heat content anomalies are similar between the ZC model and the ICM, whereas the SSTA patterns are significantly different.

The differences in the derived CNOPs in the ICM and ZC model are comprehensible. On the one hand, for the ICM used in this study, the derived CNOPs are dependent on the season. This can be related to the fact that the statistical relationship between $\tau$ and the SSTA, built up in the ICM, is seasonally varying; and the relationship between the anomalies of $T_e$ and the thermocline displacement are nonlocal, with the

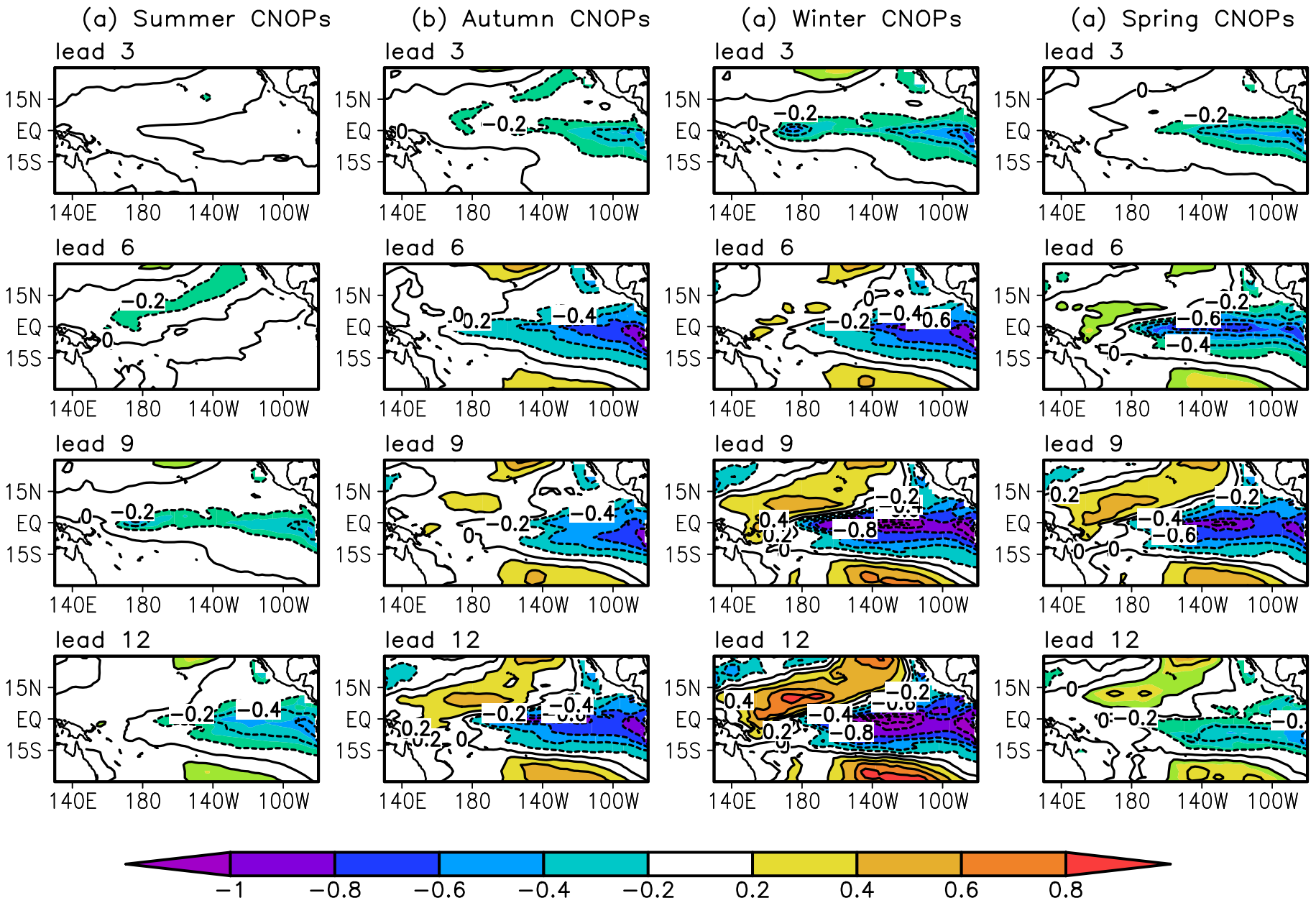


**Fig. 7.** Composite error evolutions for the SSTA component induced by (a) summer, (b) autumn, (c) winter and (d) spring CNOPs, at the initial time of August (−1), November (−1), February (0) and May (0), respectively. The contour interval is 0.2°C.

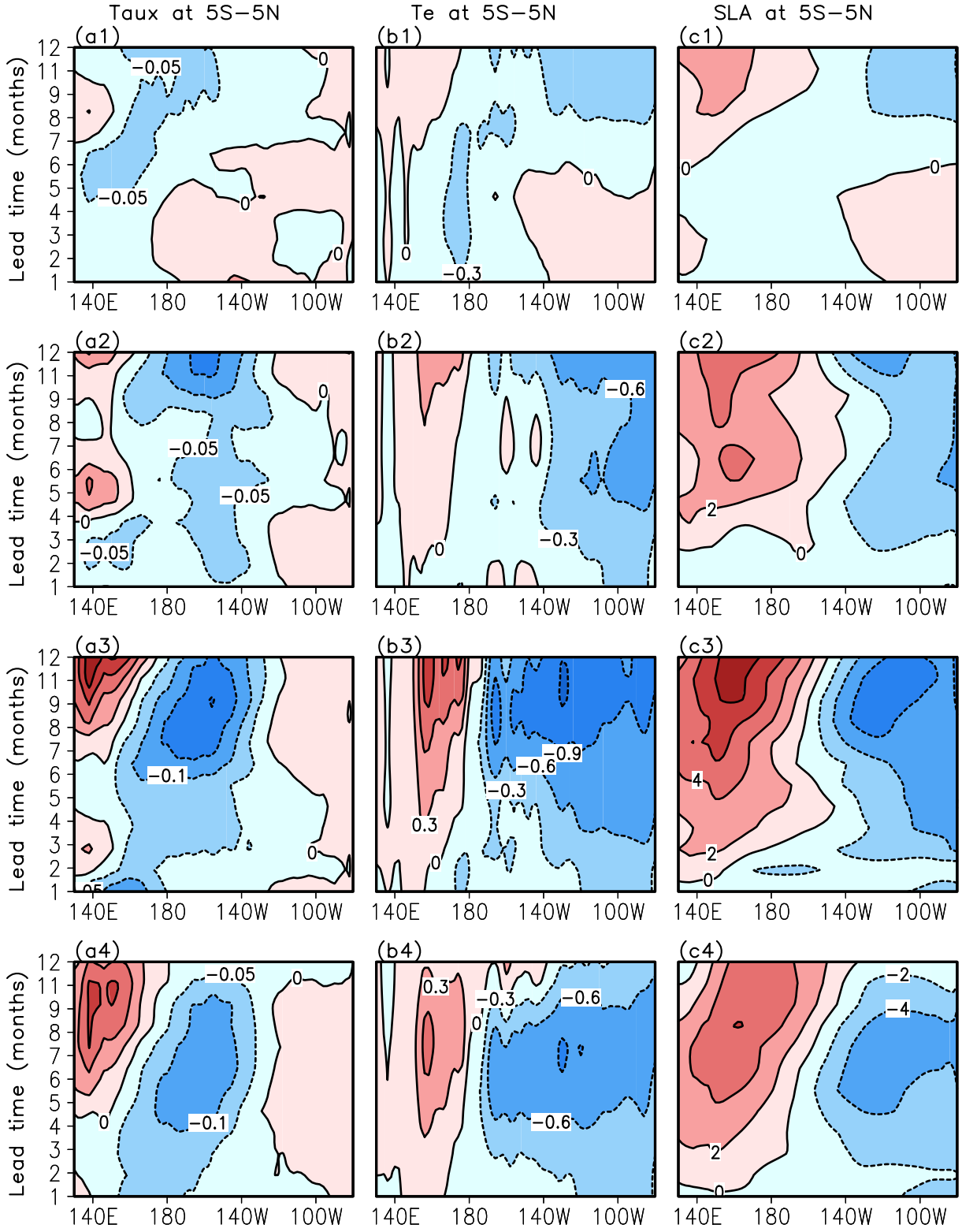


**Fig. 8.** Longitude–time sections of prediction errors along the equator (5°N–5°S) induced by CNOPs for the (a) zonal wind stress anomaly, (b) subsurface entrainment temperature anomaly, and (c) sea level anomaly. From the top row to the bottom row are the cases for summer, autumn, winter and spring CNOPs, respectively, numbered as 1, 2, 3 and 4. The contour interval is 0.05 dyn cm$^{-2}$ in (a), 0.3°C in (b), and 2 cm in (c).

largest $T_e$ anomalies centered in the central equatorial Pacific. As a result, the CNOPs in the ICM are sensitive to the start season and a large signal in the central Pacific can then propagate to the east, causing large error growth in the Niño3.4 area. Note that, in the ZC model, a local nonlinear parameterization scheme is adopted to represent the subsurface en-

trainment temperature anomaly, with the largest $T_e$ anomalies centered in the eastern equatorial Pacific; initial error growth in the ZC model tends to be localized in the east. This is the reason why the CNOPs of the SSTA in the ZC model are confined to the eastern Pacific. On the other hand, nonlinearity can be a factor enhancing the asymmetry of ENSO (An and Jin, 2004; Duan et al., 2009, 2013). Because of the adoption of a linear statistical atmospheric model and linear thermocline feedback in the ICM, the modeled ENSO is less asymmetric. This may cause the OIEs that are almost exactly the same between the onset phase and decay phase of ENSO.

Given the local distribution of large-value initial-condition errors as identified by the CNOPs, sensitive areas exist where the initial errors can cause the prediction of ENSO to deviate substantially from the real-world situation. By removing the errors in these sensitive areas, the prediction skill should improve considerably. The eastern Pacific is a suggested sensitive area in the ZC model. However, noting that the CNOPs in the ICM are season-dependent, the indication for this model is that the sensitive areas for targeted observations in ENSO prediction should be adjusted with the passing of the seasons. However, the strong signals of different seasonal SLA CNOPs and SSTA CNOPs are almost all located in the eastern Pacific and central equatorial Pacific, respectively. Thus, we preliminarily deem that the upper layer of the central equatorial Pacific and subsurface of the eastern Pacific are the most sensitive areas for El Niño prediction in the ICM. Likewise, data assimilation for SSTAs in the central Pacific or data assimilation for SLAs in the eastern Pacific could effectively improve the ICM prediction skill.

## 7. Conclusion and discussion

Initial errors and model errors are the main sources of uncertainties in ENSO prediction. To investigate the optimal errors in initial conditions that cause significant prediction uncertainties in ENSO models, the LSV method has been widely used in previous studies. Recently, Mu et al. (2003) extended the LSV method to a nonlinear dynamical system and proposed the CNOP method. In this study, we used the CNOP approach to investigate the initial errors of SST and SL that can induce the largest uncertainties in El Niño predictions in an ICM.

It was found that the CNOPs are significantly season-dependent. Four seasonal CNOPs of SSTA are demonstrated. Both the summer and winter types of SSTA CNOPs possess large-scale negative values near the dateline in the central Pacific. The spring SSTA CNOPs show a dipole pattern, with positive anomalies in the northwestern tropical Pacific and negative anomalies in the south tropical Pacific. The OIEs derived from the autumn season also exhibit a dipole pattern, with negative values in the north tropical and equatorial Pacific, and positive values in the south tropical Pacific. Meanwhile, for the four seasonal CNOP-type errors of SLA, they share the same feature of a kind of seesaw structure, with positive values in the west and negative values in the east along the line of 10°N. However, there is an evident difference in the intensity revealed in the eastern equatorial Pacific: a weak positive signal is present in summer, while a strong positive signal is present in other seasons. Note that the combinations of initial error fields induce large prediction uncertainties at 12-month lead times. Although similarities exist among the four seasonal CNOPs of SSTA or SLA, the combination of SSTA and SLA CNOPs, separately referred to as summer, autumn, winter and spring CNOPs, is significantly season-dependent.

The combined errors induced by different seasonal CNOPs are distinct: large prediction uncertainties are invoked by winter CNOPs and small error growth is induced by autumn CNOPs. Moreover, the CNOP-induced error evolution is sensitive to the calendar month, insofar as the largest error growth tendencies during prediction appear from May to September. On this point, we conclude that specific types of initial error (e.g., CNOPs) can cause the SPB phenomenon. Furthermore, we found that the CNOPs tend to evolve into La Niña-like events. This indicates that, when predicting an El Niño from initial conditions having CNOP-like errors, the model will tend to predict a weak El Niño event. The evolution of each seasonal CNOP has the same dynamics as those of ENSO, such as Bjerknes positive feedback and thermocline feedback. Details on the evolution of each season CNOP were also discussed.

Note that regions with large values of CNOPs were found to be localized, indicating that the initial errors in these regions (i.e., sensitive areas) play an important role in producing prediction errors. Given the fact that CNOPs vary with season, we further suggest that targeted observation strategies should be implemented seasonally. If data assimilation is implemented in the central Pacific for SSTAs, and in the eastern Pacific for SLAs, an improved skill in ENSO prediction should be effectively achievable in this ICM. However, more experiments need to be carried out in future work to verify this expectation.

It should be emphasized that the purpose of this study was to examine the effects induced by the initial errors on ENSO predictions regardless of the uncertainties in model parameters. In fact, despite the good performance of ENSO prediction in the ICM, the imperfections in model physics cannot be neglected in a realistic forecast (e.g., the low prediction skill in the western tropical Pacific; Fig. 1). The simulated ENSO is strongly related to certain model parameters [e.g., the relative coupling coefficient (Gao et al., 2016)], meso- and small-scale processes [e.g., tropical instability waves (Zhang and Busalacchi, 2008)], and stochastic wind forcing (e.g., Zhang et al., 2008). Flügel and Chang (1996) demonstrated that the impact of stochastic processes on a coupled ocean–atmosphere system is considerably larger than the effect of nonlinear dynamical processes on short lead-time prediction. Chang et al. (1996) suggested that stochastic forcing plays two roles in ENSO cycles: break-up phase-locking, and exciting ENSO-like variability in a stable regime. Additionally, Zhou et al. (2008) emphasized the impact of atmospheric nonlinearities on the optimal growth of prediction error; that is, the nonlinear effect of atmospheric processes be-

comes more important for a long-lead time prediction. Thus, the results obtained based on only the initial-condition errors need to be extended to include the effects of errors in model physics. In follow-up work, the CNOP approach will also be used to assess the effects of model parameters and stochastic forcing on ENSO prediction skill in the ICM. Preliminary results indicate that data assimilation in the central Pacific for SSTAs, and in the eastern Pacific for SLAs, can effectively improve the ICM's prediction skill.

***Acknowledgements.*** We would like to thank Drs. Mu MU, Qiang WANG, Wansuo DUAN, Xinrong WU, and Hui XU for their comments and help in implementing the CNOP approach into the ICM. We also wish to thank the two anonymous reviewers for their insightful comments and constructive suggestions. This research was supported by the National Natural Science Foundation of China (NFSC; Grant Nos. 41690122, 41690120, 41490644, 41490640 and 41475101), the AoShan Talents Program supported by Qingdao National Laboratory for Marine Science and Technology (Grant No. 2015ASTP), a Chinese Academy of Sciences Strategic Priority Project, the Western Pacific Ocean System (Grant Nos. XDA11010105, XDA11020306), the NSFC–Shandong Joint Fund for Marine Science Research Centers (Grant No. U1406401), the National Natural Science Foundation of China Innovative Group Grant (Grant No. 41421005), and the Taishan Scholarship and Qingdao Innovative Program (Grant No. 2014GJJS0101).

## REFERENCES

An, S. I., and F. F. Jin, 2004: Nonlinearity and asymmetry of ENSO. *J. Climate*, **17**, 2399–2412.

Balmaseda, M. A., M. K. Davey, and D. L. T. Anderson, 1995: Decadal and seasonal dependence of Enso prediction skill. *J. Climate*, **8**, 2705–2715.

Battisti, D. S., 1988: Dynamics and thermodynamics of a warming event in a coupled tropical atmosphere-ocean model. *J. Atmos. Sci.*, **45**, 2889–2919.

Birgin, E. G., J. M. Martínez, and M. Raydan, 2000: Nonmonotone spectral projected gradient methods on convex sets. *SIAM Journal on Optimization*, **10**, 1196–1211.

Bjerknes, J., 1969: Atmospheric teleconnections from the equatorial pacific. *Mon. Wea. Rev.*, **97**, 163–172.

Blumenthal, M. B., 1991: Predictability of a coupled ocean-atmosphere model. *J. Climate*, **4**, 766–784.

Chang, P., L. Ji, H. Li, and M. Flügel, 1996: Chaotic dynamics versus stochastic processes in El Niño-Southern Oscillation in coupled ocean-atmosphere models. *Physica D*, **98**, 301–320.

Chen, D. K., and M. A. Cane, 2008: El Niño prediction and predictability. *Journal of Computational Physics*, **227**, 3625–3640.

Chen, D. K., S. E. Zebiak, A. J. Busalacchi, and M. A. Cane, 1995: An improved procedure for EI Niño forecasting: Implications for predictability. *Science*, **269**, 1699–1702.

Chen, D. K., S. E. Zebiak, M. A. Cane, and A. J. Busalacchi, 1997: Initialization and predictability of a coupled ENSO forecast model. *Mon. Wea. Rev.*, **125**, 773–788.

Chen, D. K., M. A. Cane, A. Kaplan, S. E. Zebiak, and D. J. Huang, 2004: Predictability of El Niño over the past 148 years. *Nature*, **428**, 733–736.

Chen, D. K., and Coauthors, 2015: Strong influence of westerly wind bursts on El Niño diversity. *Nature Geosci.*, **8**, 339–345.

Duan, W. S., F. Xue, and M. Mu, 2009: Investigating a nonlinear characteristic of El Niño events by conditional nonlinear optimal perturbation. *Atmospheric Research*, **94**, 10–18.

Duan, W. S., Y. S. Yu, H. Xu, and P. Zhao, 2013: Behaviors of nonlinearities modulating the El Niño events induced by optimal precursory disturbances. *Climate Dyn.*, **40**, 1399–1413.

Fan, Y., M. R. Allen, D. L. T. Anderson, and M. A. Balmaseda, 2000: How predictability depends on the nature of uncertainty in initial conditions in a coupled model of ENSO. *J. Climate*, **13**, 3298–3313.

Flügel, M., and P. Chang, 1996: Impact of dynamical and stochastic processes on the predictability of ENSO. *Geophys. Res. Lett.*, **23**, 2089–2092.

Gao, C., and R. H. Zhang, 2017: The roles of atmospheric wind and entrained water temperature ($T_e$) in the second-year cooling of the 2010-12 La Niña event. *Climate Dyn.*, **48**, 597–617.

Gao, C., X. R. Wu, and R. H. Zhang, 2016: Testing a four-dimensional variational data assimilation method using an improved intermediate coupled model for ENSO analysis and prediction. *Adv. Atmos. Sci.*, **33**, 875–888, doi: 10.1007/s00376-016-5249-1.

Goswami, B. N., and J. Shukla, 1991: Predictability of a coupled ocean-atmosphere model. *J. Climate*, **4**, 3–22.

Jin, E. K., and Coauthors, 2008: Current status of ENSO prediction skill in coupled ocean-atmosphere models. *Climate Dyn.*, **31**, 647–664.

Keenlyside, N. S., 2001: Improved modelling of zonal currents and SST in the tropical Pacific. PhD dissertation, Department of Mathematics and Statistics, Monash University, Clayton, Victoria, Australia, 194 pp.

Keenlyside, N. S. and Kleeman R., 2002: Annual cycle of equatorial zonal currents in the Pacific. *J. Geophys. Res.*, **107**(C8), 3093, doi: 10.1029/2000JC000711.

Lorenz, E. N., 1965: A study of the predictability of a 28-variable atmospheric model. *Tellus*, **17**, 321–333.

Luo, J. J., S. Masson, S. K. Behera, and T. Yamagata, 2008: Extended ENSO predictions using a fully coupled ocean-atmosphere model. *J. Climate*, **21**, 84–93.

Moore, A. M., and R. Kleeman, 1996: The dynamics of error growth and predictability in a coupled model of ENSO. *Quart. J. Roy. Meteor. Soc.*, **122**, 1405–1446.

Moore, J., A. Grinsted, and S. Jevrejeva, 2009: Wavelet-lag regression analysis of Atlantic tropical cyclones. *Hurricanes and Climate Change*, J. B. Elsner and T. H. Jagger, Eds., Springer, 139–152.

Morss, R. E., and D. S. Battisti, 2004a: Evaluating observing requirements for ENSO prediction: Experiments with an intermediate coupled model. *J. Climate*, **17**, 3057–3073.

Morss, R. E., and D. S. Battisti, 2004b: Designing efficient observing networks for ENSO prediction. *J. Climate*, **17**, 3074–3089.

McCreary J. P., 1981: A linear stratified ocean model of the equatorial undercurrent. Philos Trans Roy Soc London 298: 603–635

Mu, M., W. S. Duan, and B. Wang, 2003: Conditional nonlinear optimal perturbation and its applications. *Nonlinear Processes in Geophysics*, **10**, 493–501.

Mu, M., W. S. Duan, and B. Wang, 2007a: Season-dependent dynamics of nonlinear optimal error growth and El Niño-Southern Oscillation predictability in a theoretical model. *J.*

*Geophys. Res.*, **112**, doi: 10.1029/2005JD006981.

Mu, M., H. Xu, and W. S. Duan, 2007b: A kind of initial errors related to "spring predictability barrier" for El Niño events in Zebiak-Cane model. *Geophys. Res. Lett.*, **34**, doi: 10.1029/2006GL027412.

Mu, M., Y. S. Yu, H. Xu, and T. T. Gong, 2014: Similarities between optimal precursors for ENSO events and optimally growing initial errors in El Niño predictions. *Theor. Appl. Climatol.*, **115**, 461–469.

Mu, M., W. S. Duan, D. K. Chen, and W. D. Yu, 2015: Target observations for improving initialization of high-impact ocean-atmospheric environmental events forecasting. *National Science Review*, **2**, 226–236.

Philander, S. G. H., 1983: El Niño southern oscillation phenomena. *Nature*, **302**, 295–301.

Reynolds, R. W., N. A. Rayner, T. M. Smith, D. C. Stokes, and W. Q. Wang, 2002: An improved in situ and satellite SST analysis for climate. *J. Climate*, **15**, 1609–1625.

Ropelewski, C. F., and M. S. Halpert, 1987: Global and regional scale precipitation patterns associated with the El Niño/southern oscillation. *Mon. Wea. Rev.*, **115**, 1606–1626.

Ropelewski, C. F., V. E. Kousky, and X. Wang, 1996: Precipitation-related circulation over the Americas based on reanalysis. *Eighth Conference on Air-Sea Interaction and Conference on the Global Ocean-Atmosphere-Land System* (*Goals*), 381–384.

Samelson, R. M., and E. Tziperman, 2001: Instability of the chaotic ENSO: The growth-phase predictability barrier. *J. Atmos. Sci.*, **58**, 3613–3625.

Toth, Z., and E. Kalnay, 1997: Ensemble forecasting at NCEP and the breeding method. *Mon. Wea. Rev.*, **125**, 3297–3319.

Wang, B., and Z. Fang, 1996: Chaotic oscillations of tropical climate: A dynamic system theory for ENSO. *J. Atmos. Sci.*, **53**, 2786–2802.

Wang, C. Z., and J. Picaut, 2004: Understanding ENSO physics—A review. *Earth's Climate*, C. Wang, S. P. Xie and J. A. Carton, American Geophysical Union, 21–48.

Wang, C. Z., and P. C. Fiedler, 2006: ENSO variability and the eastern tropical Pacific: A review. *Progress in Oceanography*, **69**, 239–266.

Webster, P. J., 1995: The annual cycle and the predictability of the tropical coupled ocean-atmosphere system. *Meteor. Atmos. Phys.*, **56**, 33–55.

Webster, P. J., and S. Yang, 1992: Monsoon and ENSO: Selectively interactive systems. *Quart. J. Roy. Meteor. Soc.*, **118**, 877–926.

Xu, H., 2006: Studies of predictability problems for Zebiak-Cane ENSO model. PhD. dissertation, Institute of Atmospheric Physics, Chinese Academy of Sciences. (in Chinese)

Xue, Y., M. A. Cane, S. E. Zebiak, and M. B. Blumenthal, 1994: On the prediction of ENSO—A study with a low-order Markov model. *Tellus A*, **46**, 512–528.

Xue, Y., M. A. Cane, and S. E. Zebiak, 1997a: Predictability of a coupled model of ENSO using singular vector analysis. Part II: Optimal growth and forecast skill. *Mon. Wea. Rev.*, **125**, 2057–2073.

Xue, Y., M. A. Cane, and S. E. Zebiak, 1997b: Predictability of a coupled model of ENSO using singular vector analysis. Part I: Optimal growth in seasonal background and ENSO cycles. *Mon. Wea. Rev.*, **125**, 2043–2056.

Yu, Y. S., W. S. Duan, X. Hui, and M. Mu, 2009: Dynamics of nonlinear error growth and season-dependent predictability of El Niño events in the Zebiak-Cane model. *Quart. J. Roy. Meteor. Soc.*, **135**, 2146–2160.

Yu, Y. S., M. Mu, W. S. Duan, and T. T. Gong, 2012: Contribution of the location and spatial pattern of initial error to uncertainties in El Niño predictions. *J. Geophys. Res.*, **117**, doi: 10.1029/2011JC007758.

Zebiak, S. E., and M. A. Cane, 1987: A model El Niño-southern oscillation. *Mon. Wea. Rev.*, **115**, 2262–2278.

Zhang, R. H., and A. J. Busalacchi, 2008: Rectified effects of tropical instability wave (TIW)-induced atmospheric wind feedback in the tropical Pacific. *Geophys. Res. Lett.*, **35**, doi: 10.1029/2007GL033028.

Zhang, R. H., and C. Gao, 2016: Role of subsurface entrainment temperature (Te) in the onset of El Niño events, as represented in an intermediate coupled model. *Climate Dyn.*, **46**, 1417–1435.

Zhang, R. H., L. M. Rothstein, and A. J. Busalacchi, 1998: Origin of upper-ocean warming and El Niño change on decadal scales in the tropical Pacific Ocean. *Nature*, **391**, 879–883.

Zhang, R. H., S. E. Zebiak, R. Kleeman, and N. Keenlyside, 2003: A new intermediate coupled model for El Niño simulation and prediction. *Geophys. Res. Lett.*, **30**, doi: 10.1029/2003GL018010.

Zhang, R. H., R. Kleeman, S. E. Zebiak, N. Keenlyside, and S. Raynaud, 2005a: An empirical parameterization of subsurface entrainment temperature for improved SST anomaly simulations in an intermediate ocean model. *J. Climate*, **18**, 350–371.

Zhang, R. H., S. E. Zebiak, R. Kleeman, and N. Keenlyside, 2005b: Retrospective El Niño forecasts using an improved intermediate coupled model. *Mon. Wea. Rev.*, **133**, 2777–2802.

Zhang, R. H., A. J. Busalacchi, and D. G. DeWitt, 2008: The Roles of Atmospheric Stochastic Forcing (SF) and Oceanic Entrainment Temperature ($T_e$) in Decadal Modulation of ENSO. *J. Climate*, **21**, 674–704.

Zhang, R. H., F. Zheng, J. Zhu, and Z. G. Wang, 2013: A successful real-time forecast of the 2010-11 La Niña event. *Scientific Reports*, **3**, 1108.

Zhou, X. B., Y. M. Tang, and Z. W. Deng, 2008: The impact of atmospheric nonlinearities on the fastest growth of ENSO prediction error. *Climate Dyn.*, **30**, 519–531.

Zhu, J. S., B. H. Huang, L. Marx, J. L. Kinter III, M. A. Balmaseda, R. H. Zhang, and Z. Z. Hu, 2012: Ensemble ENSO hindcasts initialized from multiple ocean analyses. *Geophys. Res. Lett.*, **39**, doi: 10.1029/2012GL051503.

Zhu, J. S., A. Kumar, and B. H. Huang, 2015a: The relationship between thermocline depth and SST anomalies in the eastern equatorial Pacific: Seasonality and decadal variations. *Geophys. Res. Lett.*, **42**, 4507–4515.

Zhu, J. S., A. Kumar, H. Wang, and B. H. Huang, 2015b: Sea surface temperature predictions in NCEP CFSv2 using a simple ocean initialization scheme. *Mon. Wea. Rev.*, **143**, 3176–3191.